9

Integrated sea surface temperature products within a coastal ocean observing system

Nadya T. Vinogradova
Atmospheric and Environmental Research, Inc. (AER)
USA

1. Introduction

Integration of regional information from existing ocean observing platforms, such as satellite and in situ observations, and from data assimilation and modelling systems is essential for our understanding and prediction of regional environments and ecosystems. The strategy of such integration is to link existing modelling and observing systems – both in situ and space-borne, - and to collect new atmospheric and ocean observations to better understand the Earth system, to monitor the climate, to predict environmental changes and mitigate natural disasters. Remarkable progress has been made in recent years toward the establishment of a global Earth observing system. As a result of an international June 2003 G8 Heads of State meeting, the U.S. Integrated Ocean Observing System (IOOS) was created, as a part of the Global Earth Observing System of Systems (GEOSS). The system is a pioneering architecture that provides new observational capabilities to advance informed decision making on national, regional, and local levels. The IOOS development plan (http://www.ocean.us./ioospln.jsp) called for both global and regional components. The coastal component consists of regional coastal observing systems that engage a broad spectrum of data providers and users who can depend on operational systems with the capacity to rapidly detect and provide timely predictions of changes occurring in the coastal environments.

One of the most essential variables in ocean dynamics that is used to monitor climate change is sea surface temperature (SST). Variations in SST are important indicators of climate variability, and can be related to other climate variables, such as sea level change, hurricane intensity, and air-sea fluxes of CO_2. In addition, SSTs are widely used in ocean modelling efforts by providing surface boundary conditions and/or observational constraints for atmospheric and oceanic hindcasts and forecasts. To increase resolution and to improve quality of analysis, SST products are often constructed by combining measurements from a variety of sources. Examples of global, operational, satellite SST products include the Global Ocean Data Assimilation Experiment (GODAE) High-Resolution SST Pilot Project (GHRSST-PP) (Donlon et al., 2007), NOAA/NASA Advanced Very High Resolution Radiometer (AVHRR) Pathfinder SST analyses (Reynolds et al., 2002), Tropical Rainfall Measuring Mission (TRMM) Microwave Imager (TMI) and NASA Advanced Microwave

Scanning Radiometer (AMSR) SST products (Chelton & Wentz, 2005). A list of available operational GHRSST products is given in Table 1.

SST product name	Satellite sensors used	Agency Identifier	Grid Spacing	Period
OYSSEA	AVHRR, AMSRE, TMI, AATST, SEVIRI, GOES	CNES IFREMER	6 km	Day 274 2007 - present
AVHRR_OI	AVHRR, in situ	NOAA	0.25°	1985 - present
AVHRR_AMSR_OI	AVHRR, AMSRE, in situ	NOAA	0.25°	Day 152 2002 - present
OSTIA	AVHRR, AMSRE, TMI, AATSR, SEVIRI, in situ	UK Met Office	5 km	April 2006 - present
MW_IR_OI	AMSRE, TMI, MODIS	Remote Sensing Systems	9 km	Day 233 2005 - present
NAVO K10	AVHRR, GOES, AMSRE	NAVOVEANO (NAVY)	10 km	Day 92 2008 - present

Table 1. Examples of available daily global SST analyses provided by GHRSST group

The products are typically based on merged, optimally-interpolated multi-sensor SST data sets. All these products are high-quality, high-resolution, daily global analyses that also provide the errors associated with their interpolation procedure. For example, Ocean Surface Temperature and Ice Analysis (OSTIA), provided by the UK Met Office (see example in Figure 1), is generated globally in near-real time on a 1/20° (~5-km) grid and is routinely validated using independent observations from Marine-Atmospheric Emitted Radiance Interferometer (M-AERI). The system combines satellite microwave and infrared measurements with in situ observations from ships and buoys using optimal interpolation with correlation length of 700 km, and it has a root-mean-square error within 0.8 °C. (Stark et al., 2007). Another example of the real-time global SST analyses (RTG_SST) is shown in Figure 2. The fields are developed at the National Centres for Environmental Prediction (NCEP) on a 1/12° (~9-km) grid as a blend of in situ and AVHRR observations using variational analysis with isotropic correlation scales that vary from 100 km in areas of high temperature gradients to 450 km in areas of low SST gradients (Thiébaux et al., 2003). Comparison with buoy data resulted in average root-mean-square error within 1 °C.

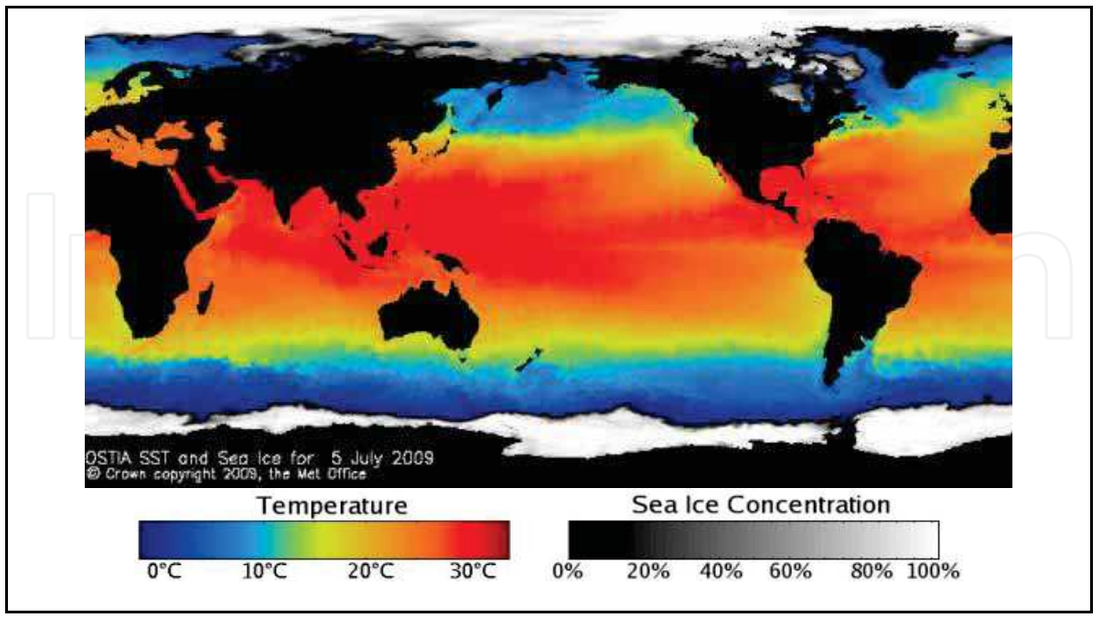

Fig. 1. OSTIA analysis: An example of integrated SST product based on synthesis of infrared and microwave satellite-derived SSTs with in situ data on July 5 2009 in °C. Spatial resolution ~5 km. Source: UK Met Office website

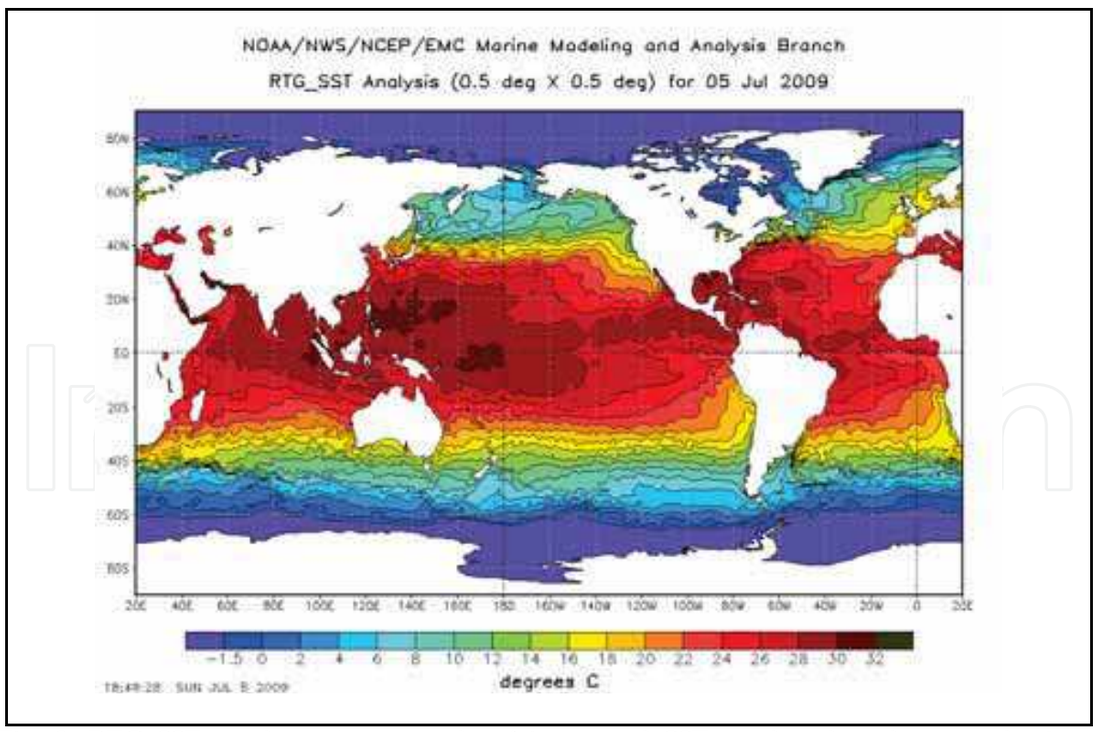

Fig. 2. RTG_SST product: An example of integrated SST product based on synthesis of infrared satellite-derived SSTs with in situ data on July 5 2009 in °C. Spatial resolution ~9 km. Source: NCEP website.

Another source of integrated high-quality SST analyses are solutions provided by general ocean circulation models. Ocean models provide an estimate of the ocean state, including SST, that could be constrained by observations and the model physics and that approximates the time evolution according to the model's equations and parameterizations of the fluxes. Observational constraints range from satellite-derived SST fields (e.g., GoMOOS model, Xue et al., 2005) to almost all available ocean datasets including in situ and satellite-derived observations such as altimetry, Argo, CTD, XBT, scatterometer, SST, SSS, etc. (e.g., ECCO-GODAE solution, Wunsch et al., 2009). Ocean models are typically fit in a least-squares sense to each datasets, each weighted according to the best existing estimate of the data and model errors (see Section 2 for more details). Such combinations provide optimal estimates, given model physics and knowledge of the data. Evaluation of how well model solution fits the data is usually done in terms of cost ratio, which is defined as the variance of model-data differences divided by data error variance:

$$\text{cost} = \frac{\langle M - D \rangle^2}{\sigma^2_{DATA}} \tag{1}$$

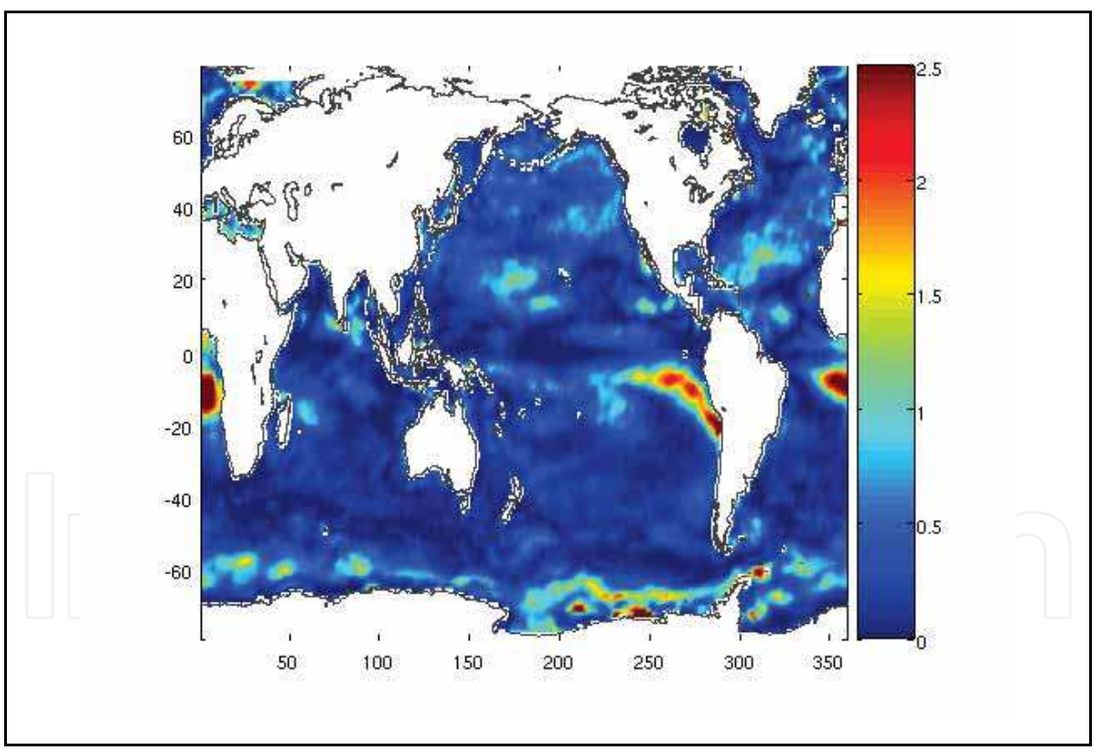

Fig. 3. Example of the cost calculated according to equation (1) for the global ECCO-GODAE model solution and GHRSST-AVHRR_OI product at annual frequency. ECCO-GODAE optimization is achieved in terms of minimizing the model/data differences. The example above shows consistency between the model and data seasonal cycles, which is the dominant signal in SST variability. Values of the cost that are close or less than one indicate good model/data agreement within the noise level of the data. The optimization of the

ECCO products is still ongoing, but overall there is a good agreement between the solution and SST data within the expected noise level.

A well-constrained model solution typically has values of the cost that are close to one, indicating a good model/data agreement within the noise level of the observations (see example in Figure 3).

2. Integration methods

Each of the two integration approaches mentioned above, i.e. pure data synthesis and model/data integration, has both advantages and limitations. For example, infrared measurements (AVHRR, MODIS) allow higher spatial resolution, especially in coastal areas, but they can be less accurate than microwave data (AMSR, TMI) due to cloud contaminations. In addition, blended analyses tend to over-smooth ocean fine spatial structures, such as fronts and eddies (Donlon et al., 2004). The products are also sensitive to methods that are chosen to blend SST datasets from different sensors, with differences between analysis reaching 2 °C. Ocean models can provide SST estimates that are physically consistent with the dynamical and thermodynamical constraints, but can also introduce additional model errors related to unresolved physics (e.g., sub-grid parameterizations).

When integrating SSTs from different sources, including blended analyses or data assimilation into numerical models, one has to estimate the total error necessary to compute the weights for synthesis algorithms. Consider the problem of estimating the model field M from data D, which measures the ocean variable with some error:

$$D = HM + \sigma_{DATA} \tag{2}$$

where H is mapping matrix that establishes the relationship between M and D. The Bayesian maximum likelihood approach (Vinogradova et al., 2005) allows one to build the optimal field that maximizes the conditional probability of the field M:

$$p\left(M|D\right) \rightarrow \max \tag{3}$$

Maximization of conditional probability can be expressed in terms of cost function J with respect to M:

$$J(M) = -\log p\left(M|D\right) = -\log p\left(D|M\right) - \log p(M) \rightarrow \min \tag{4}$$

Assuming that the errors are uncorrelated and the statistics are Gaussian, the probability density $p(D|M)$ can be expressed in terms of the data error statistics:

$$-\log p\left(D|M\right) = -\log p\left(\sigma_{DATA}\right) = -\log p\left(D - HM\right) = \left[D - HM\right]^T W \left[D - HM\right] \tag{5}$$

where T denotes transposed matrix, and W is a weight matrix, which is inversely proportional to the error covariance of data error:

$$W = \frac{1}{\sigma^2_{DATA}} \tag{6}$$

Assuming that observational errors are uncorrelated, one can estimate the data error as the difference between the data variance and model/data covariance:

$$\sigma^2_{DATA} = \left\langle D^2 \right\rangle - \left\langle MD \right\rangle \tag{7}$$

As seen from procedure (2)-(7), integration occurs within expected uncertainties of each dataset. Accurate characterization of uncertainties, or data errors σ^2_{DATA} in equation (7), is important when fitting the data to model or blending data from different sources. If the uncertainties are overestimated, one discards and loses information stored in the data. If, on the other hand, the errors are underestimated, the model is fitting noise. Figure 4 shows an example of SST error calculations that follow the procedure (2)-(7) for the North Atlantic region (Vinogradova et al., 2008). These SST errors are computed from the ECCO-GODAE ocean state estimates and global blended Reynolds OI.v2 SST analysis over the last decade. Annual signal has been removed from both model and observations. As seen from Figure 4, areas of high variability, such as western boundary currents (Gulf Stream in Figure 4), are characterized by large errors, indicating larger uncertainties in model and data. In these regions, the integration procedure will assign smaller weight to avoid imposing erroneous variability and noise fitting.

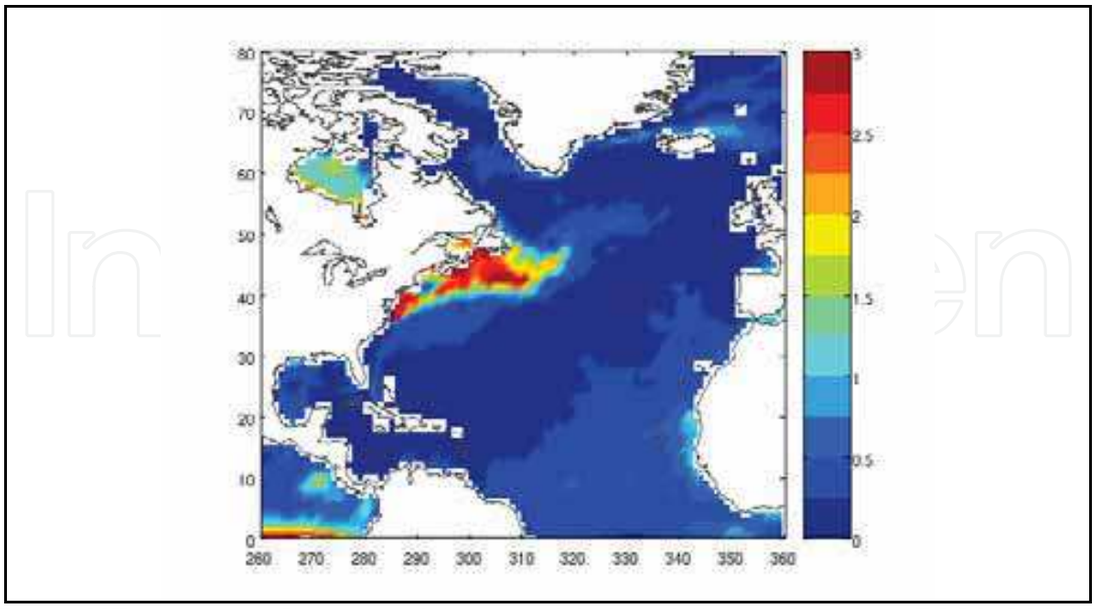

Fig. 4. SST errors (in °C) estimated from model/data difference based on ECCO-GODAE ocean state estimate and Reynolds SST analyses following the procedure (2)-(7). Annual

signal is removed. SST values in the areas with large errors will be integrated with smaller weights to avoid noise fitting.

3. Integrated SST products in coastal oceans

3.1 Integration of observations from various ocean-observing platforms.

Traditional blended SST products, described in the previous sections, are typically available as daily fields as they are based on measurements from polar-orbiting satellites which do not resolve high-frequency signals. However, high-frequency varations, and the diurnal cycle in particular, are important characteristics of the coupled atmosphere-ocean dynamics. The diurnal cycle has substantial implications in numerical weather prediction (NWP) and ocean models. Driven by solar forcing, it directly affects SST variations, the air-sea heat transfer regime, and variations in depth of the upper ocean mixed layer (Stuart-Menteth et al., 2003). Geostationary satellites, such as NOAA Geostationary Operational Environmental Satellite (GOES), provide a continuous stream of environmental data, which can be used to retrieve SST fields with high frequency. Combining observations from geostationary and polar-orbiting satellites allows one to produce a synthesized product with high spatial and temporal resolution. Presented here is an example of such regional application for the North Eastern US coast and Atlantic Canada, which is typically referred to as the Gulf of Maine region (see Figure 5).

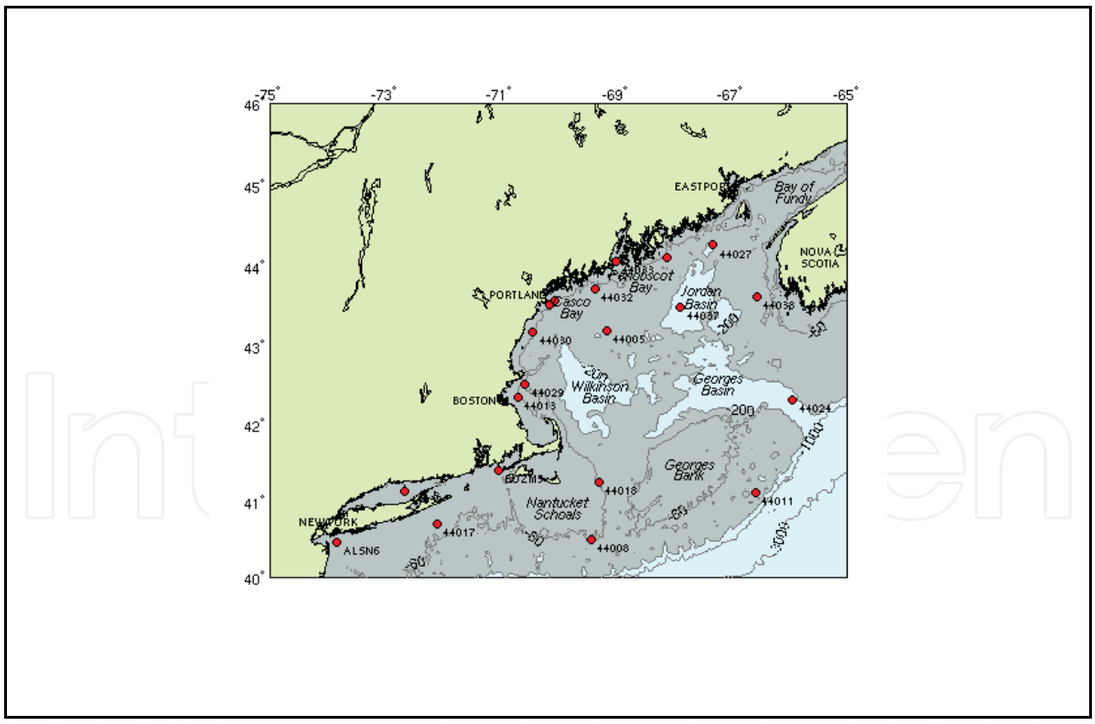

Fig. 5. The Gulf of Maine area, stretching along the coastline of New England and Atlantic Canada. The locations of the buoy stations transmitting in situ SST measurements in real time are shown as red circles. Bottom topography featuring banks and ridges is shown as contour lines.

This part of the ocean is a biologically productive and economically importtant area that covers about 92,000 km² of the ocean surface. It has a complex bottom topography, which includes banks, ridges, and basins, and extends up to 500 m deep and about 300 km offshore. From a modeling standpoint, the Gulf of Maine is a challenging area due to highly variable surface forcing, strong shelf and open ocean fluxes, and large tidal signal. The ocean circulation is mostly cyclonic and it is predominantly controlled by atmospheric heating and cooling, wind, river runoff, Scotian Shelf inflow, Gulf Stream warm-core ring intrusion and tidal mixing (Xue et al., 2000). For a successful operational forecast of the Gulf of Maine circulation, it is crucial to introduce accurate, high-resolution SST fields into a model, through data assmilation and surface boundary conditions. A synthezied AER-SST product with high spatial and temporal resolution has been developed (Vinogradova et al., 2009) to meet the demand in precise SST forcing. The fused SST product combines three sources: global temperatures estimates from (i) OSTIA and (ii) RTG_SST, described in the previous sections, and (iii) GOES radiances.

GOES SST retrievals are derived from the brightness temperatures of the GOES imager mid-wavelength infrared channel 2 at 3.9 μm and long-wavelength thermal infrared channel 4 at 10.8 μm using the AER cloud-mask detection algorithm (Gustafson et al., 2000). The cloud detection algorithm constructs a binary cloud mask using a set of multispectral tests to detect the presence of various cloud signatures. The cloud mask algorithm detects highly reflective terrain, including sun glint from water surfaces during daytime conditions using visible and thermal IR channels. The thermally-distinct cloud test compares brightness temperatures with the GFS NWP surface temperatures to detect obvious mid- and high-level clouds. The algorithm combines the results of the individual background and cloud tests to create the cloud mask. The algorithm assigns a binary cloudy/clear determination value if at least one of the cloud tests returns a positive result and all of the background tests return a negative result. After cloud mask has been applied, GOES radiances are converted to SST values following the current NOAA GOES operational SST equation:

$$SST = a_0 + a_0' S + \left(a_2 + a_2' S\right) T_2 + \left(a_4 + a_4' S\right) T_4 \tag{8}$$

where S is the satellite zenith angle,

$$S = \sec(\theta) - 1 \tag{9}$$

T_2 and T_4 are brightness temperature of channel 2 and channel 4, respectively (Maturi et al., 2007). The NOAA retrieval coefficients a_i and a_i', are listed in Table 2 and are derived from the regression analysis by matching satellite measurements with global drifting buoy observations from the Global Telecommunication System (GTS).

Imager channel	Wavelengh , μm	a_i	a_i'
0	-	-2.1000	-1.1500
2	3.78-4.03	1.1177	0.0073
4	10.2-11.2	-0.1620	-0.0690

Table 2. Retrieval coefficients for the NOAA-GOES-12 SST algorithm (from Maturi et al., 2007). The coefficients are used to convert GOES radiances to SST values.

Although GOES radiances are collected every 30 minutes, individual GOES-SST retrievals are usually contaminated by clouds. To increase spatial coverage of the retrieved GOES SSTs, the fields are averaged over the set of eight analyses. The four-hour average provides a better spatial coverage and still resolves the diurnal cycle that could be significant in the coastal dynamics. The example of the input data sources is shown in Figure 6.

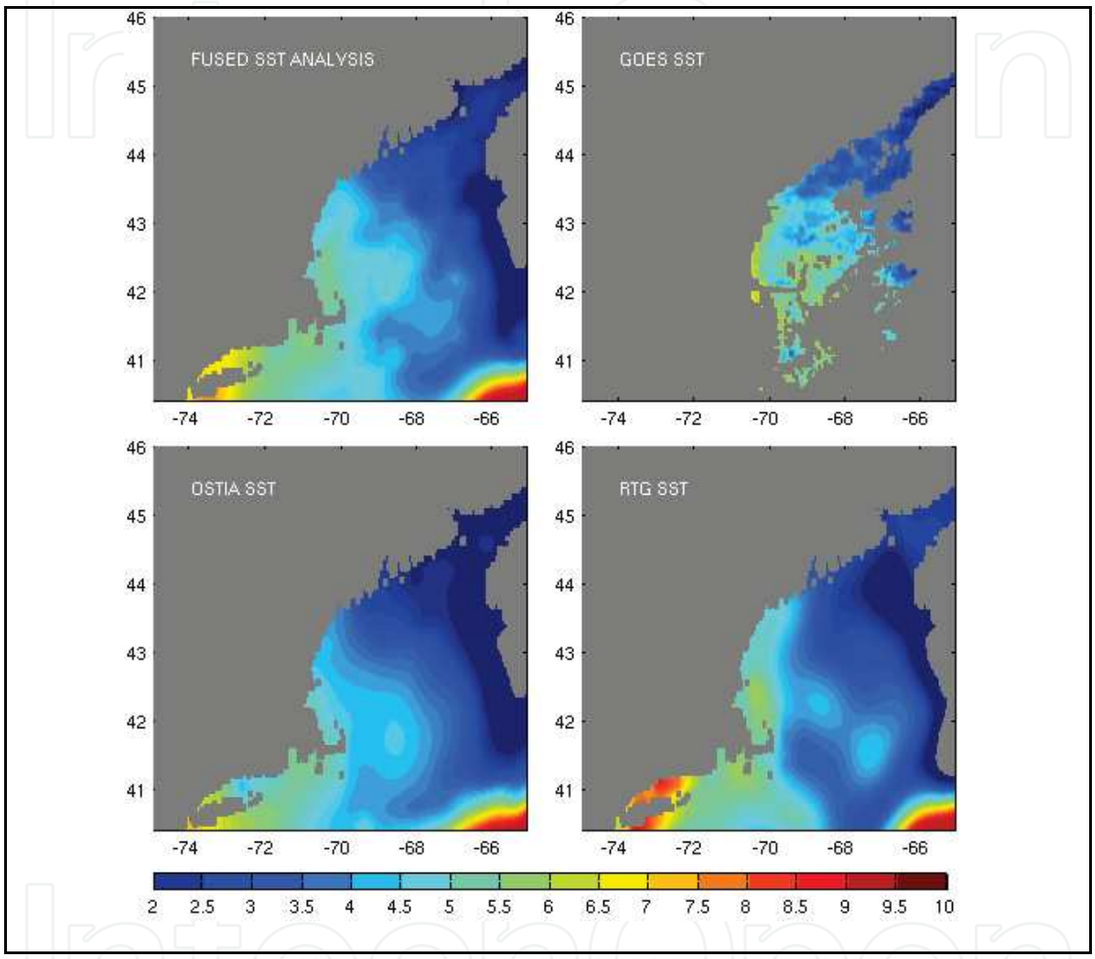

Fig. 6. Example of the SST data sources (GOES, OSTIA and RTG_SST) and fused SST analyses on May 2, 2007 in °C. Notice over-smoothed frontal features in OSTIA and RTG analyses, and unresolved cloud-contaminated coastal regions by the GOES.

Before blending, all data sets are mapped into the GOES domain (4 km) and are quality contolled to avoid artifical errors. The synthesized SST is computed as a weighted average of the three datasets with the weights being inversely proportional to the errors of each data constraint. The errors for each data sets E_i are determined by using the network of in situ SST measurments, that includes about 20 real-time buoys in that area. That allows one to assign time-varying weights, which are recomputed at every run of the system. For each data source, the errors are estimateded as a mean difference between the in situ measurment and collocated satellite SST:

$$E_i(t) = \overline{\left(D_i(t) - B(t)\right)_p} \tag{10}$$

where $i = 1,2,3$ represent each data source , D_i , $p = 1..20$ are locations of the buoys B_p , and $\overline{(.)}$ denotes spatial averaging.

To resolve diurnal variability, the analysis runs four times per day and ingests observations receieved in the preceding (?) four hours, for both in situ and satellite data. Finally, the blended solution is smoothed by its variance with the correlation scale of 10 km, which is close to the Rossby radius in this area (Xue et al., 2000). The algorithm has been implemented into a prototype near-real time production system that, since May 2007, has been producing SST fields four times a day on a 4-km grid (see example in Figure 7).

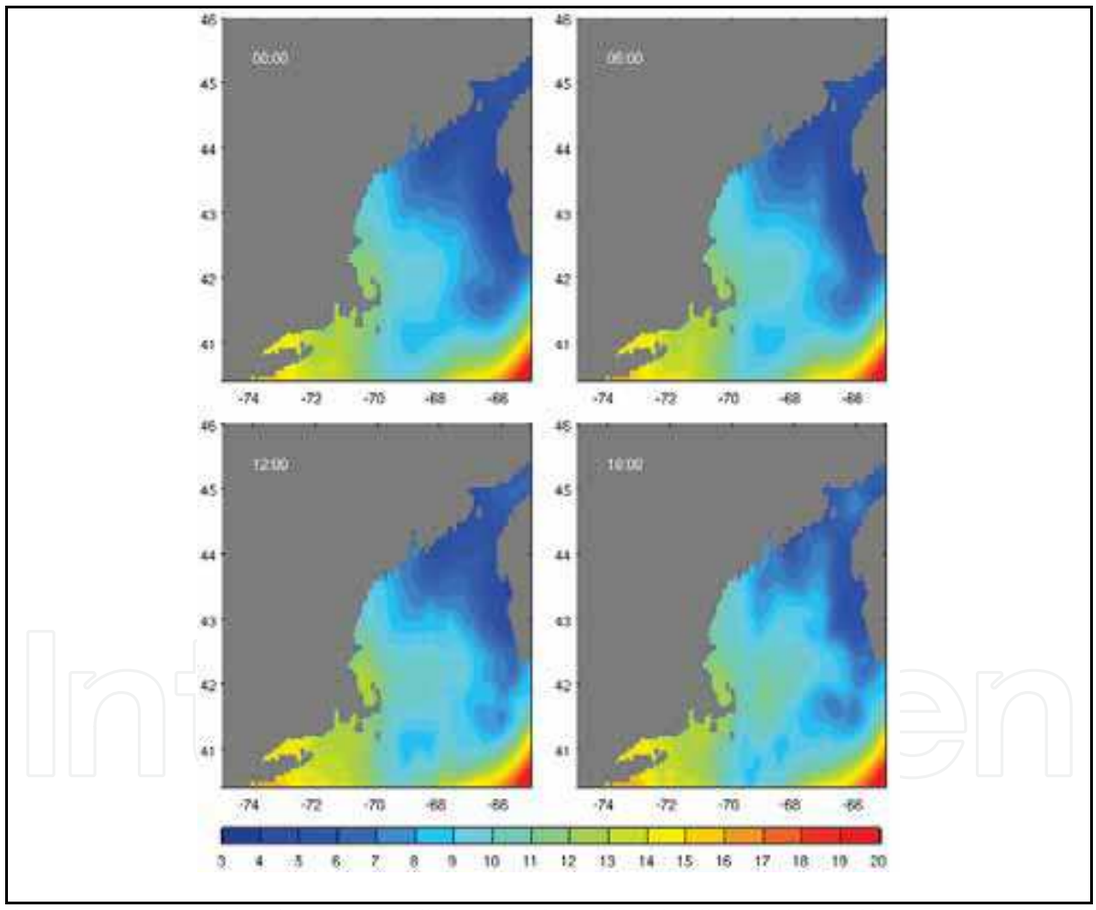

Fig. 7. Example of the fused AER-SST analysis at 00, 06, 12, and 18 UTC on June 8, 2007 in °C. The system resolves typical summer-time patterns with warmer water in the west and cooler water in the east. Other distinctive features include a strong tidal mixing front in the Georges Bank area; warm slope water intrusion in the southwest; cold water in the north-west and Bay of Fundy due to vigorous mixing in response to nearly resonant semi-diurnal tides; and cold temperature along the Maine coast resulting from summer upwelling.

The system is routinely validated by comparing the values of the blended SST analysis with in situ measurements from buoys. The average bias in the domain is found to be 0.02±0.8 °C. SST bias is attributed to bulk correction and partly to the bias of the retrieved GOES SSTs. One way to reduce the bias would be to fine-tune the regression coefficients that are used in the retrieval algorithm in the equation (1) using regional observations instead of the global match-ups. Another way to enhance system performance might be the use of the preceding improved SST synthesis as a background field instead of the daily OSTIA and RTG_SST analyses.

The ability of the AER-SST product to resolve diurnal variations has important implications in ocean studies. Many coastal regions, especially Gulf of Maine area, are well-known for strong high-frequency signals, including diurnal and nearly resonant semi-diurnal tidal responses. Tides affect not only the high-frequency spectrum, but also variability at longer periods though tidal mixing and nonlinear rectification (Xue et al., 2000). One of many possible applications of the AER-SST system is to evaluate the spatial pattern of a diurnal cycle. An example of the monthly mean diurnal cycle is shown in Figure 8. Amplitudes of diurnal variations can reach up to 2-4 °C in summer time and are attributed to high variability of the shortwave insolation that can range from 0 at night to over 900 W/m^2 at noon (Chen et al., 2003). Large-amplitude diurnal fluctuations suggest that the diurnal forcing is significant and it should be accounted for in ocean models that currently assimilate daily SSTs and do not resolve higher frequency variability. Improved high-resolution regional SSTs would also enhance estimation of the surface heat flux, which is known to play a dominant role in seasonal coastal circulation. Furthermore, knowing diurnal amplitudes will allow one to validate empirical models that are used to retrieve daytime and nighttime satellite sea-surface temperatures (Gentemann et al., 2003).

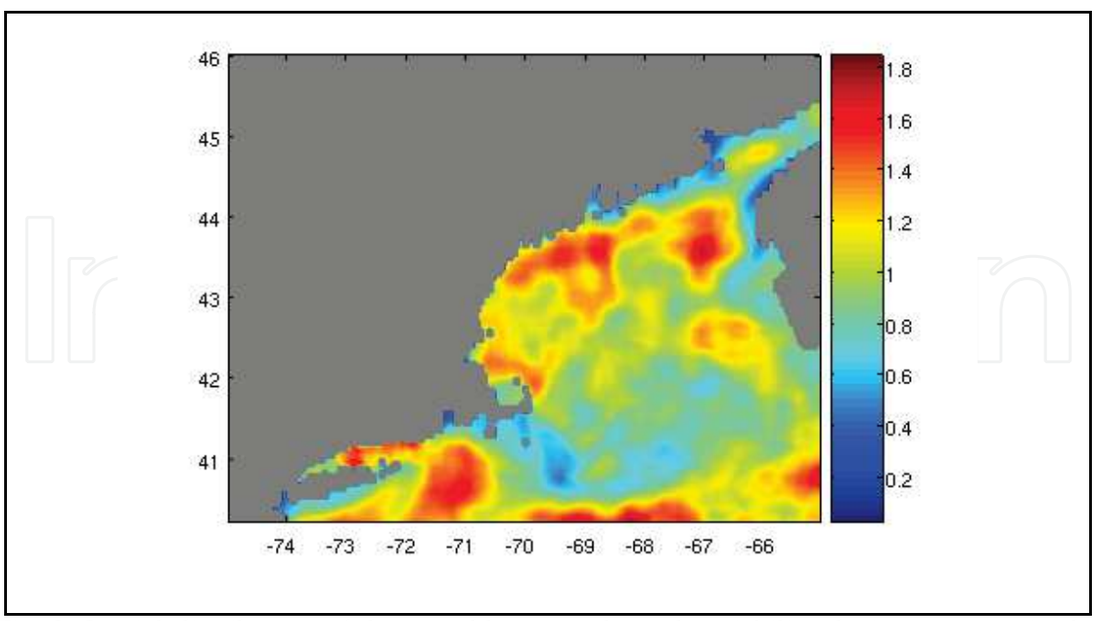

Fig. 8. Spatial distribution of the monthly mean diurnal variability during summer in the Gulf of Maine based on the AER-SST analysis (in °C).

Area-integrated value is about 2 °C, but the extreme amplitude can reach 4 °C. Complex spatial patterns are influenced by geometry of the domain and physical processes that control ocean circulation. Large values of diurnal variation are found along the coast, and in stratified and frontal regions. In the mixed regions, the diurnal cycle is weaker (e.g., the interior of the Georges Bank; western Nova Scotia). Even though solar heating increases during summertime, the buoyancy input is not strong enough compared to vigorous tidal mixing, which keeps the water well mixed and relatively cool in summer. In the stratified and frontal regions, heat is not transferred vertically as efficiently, and surface waters are more prone to diurnal warming, yielding large values of diurnal variability.

3.2 Integration of observations with ocean models

As shown in the previous section, integrated datasets based on pure observations, both satellite-derived and in situ, are useful tools to characterize upper ocean variability as a function of time and space. These products, however, do not explain the mechanisms controlling the observed variability. To interpret the observations, it is useful to analyze the equations defining an evolution of the sea surface temperature, which are also referred to as budget equations. Analysis of ocean surface heat budgets has been addressed both locally and regionally using in situ observations (Wang and McPhaden, 2001; Kim et al., 2006), and globally using theoretical calculations (Gill and Niiler, 1973). A prerequisite of a complete budget analysis is the closure of the budget, meaning that the sum of the budget components exactly matches the property tendency. Such a prerequisite is very difficult to fulfil when using raw observations and, in many cases, even numerical models (Qui, 2002). ECCO-GODAE is one of a few integrated data/model systems that allows computing closed budgets for any prognostic variable, due to consistency of the solution with the model equations and atmospheric forcing as the optimization is achieved through adjustments of the forcing fields and initial conditions. Closed property balances can be used for interpretation of the observed signals and in diagnostics of the SST tendencies, as they relate to advective and diffusive heat fluxes, or atmospheric forcing.

To characterize SST variations in terms of dynamic and thermodynamic processes that drive SST tendencies, it is useful to evaluate the strength of different terms in SST (or surface heat) balance. According to the heat content equation, the rate of change of heat storage in the surface layer occurs due to the advection and diffusive fluxes of heat, and the absorption and radiation of energy through the ocean surface:

$$\rho_0 C_p h \frac{\partial T}{\partial t} + \nabla \cdot \left(\rho C_p h T \vec{u} \right) = \nabla \cdot \left(\rho C_p h \vec{K} \right) + \frac{\partial Q}{\partial \xi} \tag{11}$$

where T is the temperature, $\vec{u}$ is the velocity vector, $\vec{K}$ is the diffusive heat flux vector, ξ is the vertical coordinate, ρ_0 is constant density of seawater, C_p is the specific heat capacity, and h is the thickness of the surface layer. Analysing the budget (11) provides information about the contribution of each term into surface heat or temperature tendency, where and when one regime is dominant over the other, and how it can be linked to ocean-

atmosphere coupling and predictability. Comparing ratios of each budget term to the total tendency can determine the extent to which each process affects surface heat content. Budget analysis by Vinogradova et al. (2008a) suggests that, in the Northern Atlantic, and in particular in the Gulf of Maine area, seasonal SST tendencies are one of the largest over the globe and can reach the values of 80 W/m² (see Figure 9). These studies also indicate that overall SST tendency due to advection is several times smaller compared to other terms, and except large scales, total tendency is a balance between surface mixing and heat fluxes across the air-sea interface.

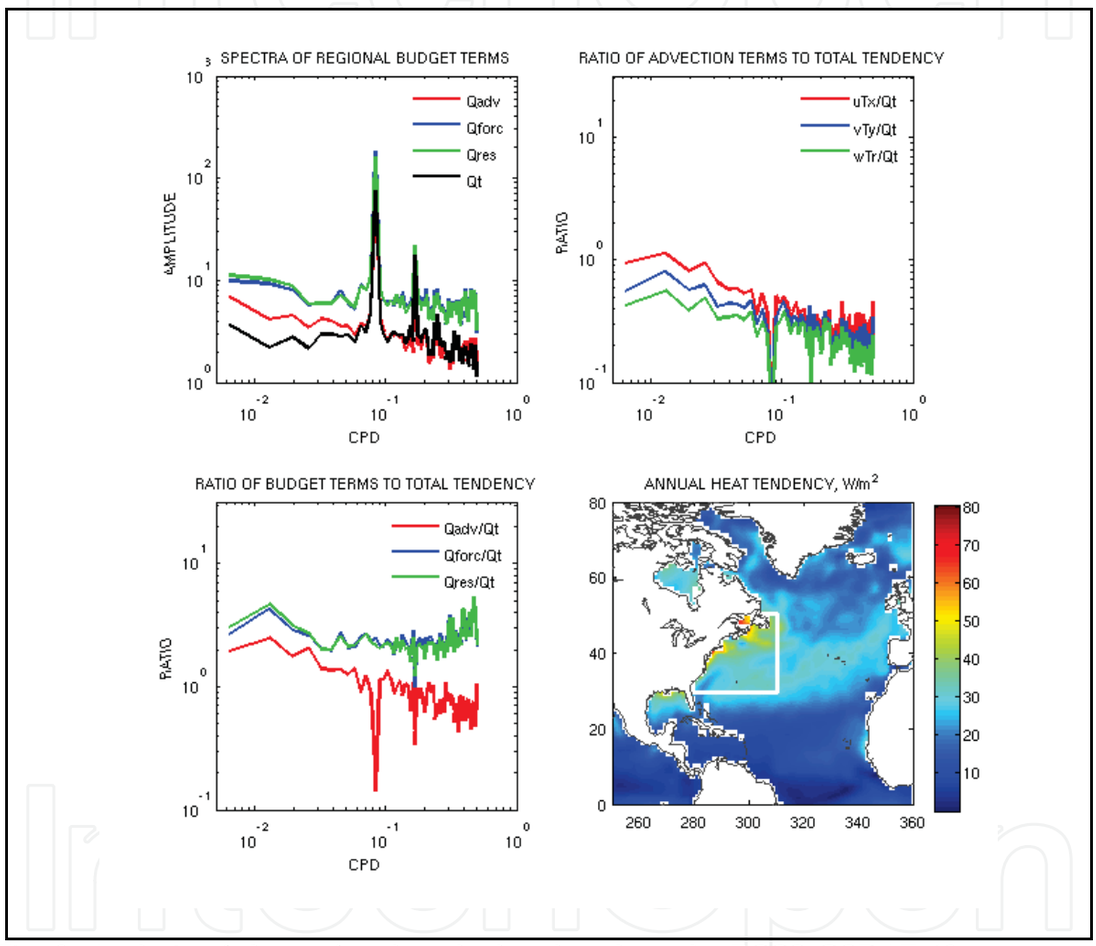

Fig. 9. Analysis of the surface heat budget based on the ECCO-GODAE 13-year ocean estimate for the North Atlantic and the Gulf of Maine area. The terms are computed according to equation (11). The ratios illustrate importance of forcing, advective and diffusive fluxes at different timescales. To analyse dynamical causes of the SST variation, advective fluxes are further evaluated in terms of meridional, zonal and vertical contributions. Along the western boundary, ratios of zonal and meridional components closely follow each other due to angular direction of the Gulf Stream. Vertical advection is generally the smallest term, but it becomes important on the decadal scales. Overall, SST tendency in this region is a balance between the diffusive fluxes and fluxes of heat across the air-sea interface.

4. Conclusion

Combinations of the advantages of the existing observing systems as well as integration of the observations into data assimilating systems provide invaluable tools for environmental management and control in the coastal regions. The need of high-quality, high-resolution SST fields, as one of the essential variables describing climate variability, has been receiving considerable attention in oceanic and atmospheric studies. With the abundance of the SST measurements, many products are based on synthesis of various data sources to produce an analysis with improved resolution and quality. Integration of SST measurements from polar-orbiting and geostationary satellites as well as in situ measurements from oceanic buoys, such as AER-SST product (Vinogradova et al., 2009), produces a new blended estimate with high spatial and temporal resolution. High temporal and spatial resolution of the system allows one to monitor fine ocean structures such as coastal fronts, describe high-frequency oceanic variability and improve regional numerical weather prediction systems. Such systems represent new coastal oceanic and atmospheric products to gain understanding and to improve prediction of the regional environment.

Integrating SST observations with data assimilating ocean numerical models provides best estimates of ocean state, given model physics and knowledge of the data. Integrated systems such as ECCO-GODAE typically continue to evolve and improve as new information (including new data and associated error estimates) becomes available. A considerable advantage of model/data integration is the ability to interpret observed variability as a function of space and time. In particular, understanding the dynamics and forcing of the SST variability is important to determine coupling mechanisms and predictability of the ocean-atmosphere system. By evaluating the prognostic equation for temperature, one can characterize the SST dynamics as a function of timescale and as function of season, which can both affect what physical mechanisms are most relevant (Vinogradova et al., 2008a). One can also differentiate between the regimes where the ocean is mostly affected by local atmospheric forcing, and those where response involve geostrophic and ageostrophic advection processes (Vinogradova & Ponte, 2009).

Identifying and understanding ocean coastal dynamics is one of the major tasks of the Integrated Ocean Observing System. Coastal oceans are highly populated areas of considerable interest to marine commerce, human recreation, oil and gas exploration and development, and are an integral part of the national and international economies. Operational integrated SST products that combine data and/or numerical models help to address important oceanographic problems of air-sea interaction and ultimately improve coastal monitoring and predictability.

5. References

Chelton, D. B. & Wentz. F. J. (2005). Global microwave satellite observations of sea surface temperature for numerical weather prediction and climate research, *Bull. Amer. Meteor. Soc.*, 86, 1097-1115.

Chen, C.; Beardsley, R. C., Franks, P. J. S., & Keuren, J. V. (2003). Influence of diurnal heating on stratification and residual circulation of Georges Bank. *J. Geophys. Res.*, 108, 8008, doi:10.1029/2001JC001245

Donlon et al. (2007), The GODAE High Resolution Sea Surface Temperature Pilot Project (GHRSST-PP), *Bull. Amer. Meteor. Society,* 88 (8).

Donlon, C. J.; Nykjaer, L., & Gentemann, C. L. (2004). Using seas surface temperature measurements from microwave and infrared satellite measurements. *International J. Remote Sensing*, 25, 1331-1336.

Gentemann, C. L.; Donlon, C. J., Stuart-Menteth, A., & Wentz, F J. (2003). Diurnal signals in satellite sea surface temperature measurements. *Geophys. Res. Lett*., 30, 1140, doi:10.1029/2002GL016291

Gustafson, G. B.; D'Entremont, R., Collins, J., & Cady-Pereira, K. (2000). VIIRS Algorithm Theoretical Basis Document (ATBD) for the Cloud Cover/Layer EDR, version 1.3

Kim, S-B.: Lee, T., & Fukumori, I. (2007). Mechanisms controlling the interannual variation of mixed layer temperature averaged over the Niño-3 region. *J. Clim.*, 20, 3822-3843.

Maturi, E.; Merchant, C., Harris, A., Li., X., & Potash, B. (2007). Geostationary sea surface temperature product validation and methodology. *Proceedings of 23th International Conference on Interactive Information and Processing Systems for Meteorology, Oceanography, and Hydrology*, San Antonio TX, January 2007

Qiu, B. (2002). The Kuroshio Extension system: its large-scale variability and role in the midlatitude ocean-atmosphere interaction. *J. Oceanography*, 58, 57-75

Reynolds, R. W.; Rayner, N. A., Smith, T. M., Stokes, D. C. & Wang, W. (2002). An improved in situ and satellite SST analysis for climate, *J. Clim*., 15, 1609-1625.

Stark J. D.; Donlon, C. J., Martin, M. J. & McCulloch. M. E. (2007). OSTIA: And operational high resolution, real time, global sea surface temperature analysis system. *Proceedings of Oceans MTS/IEEE Conference*, Vancouver, Canada. September-October 2007.

Stuart-Menteth A. C.; Robinson, I.S., & Challenor, P. G. (2003). A global study of diurnal warming using satellite-derived sea surface temperature, *J. Geophys. Res*., 108, 3155, doi:1029/2002JC001534.

Thiébaux, J.; Rogers, E., Wang, W., & Katz, B. (2003). A new high-resolution blended real-time sea surface temperature analyses. *Bull. Amer. Meteor. Soc*., 84, 645-656.

Vinogradova N. T.; Zaccheo, T. S., Alcala, C. M. & Vandemark, D. (2009). Operational high-resolution sea surface temperature product in the Gulf of Maine. *Journal of Operational Oceanography, in press.*

Vinogradova N. T.; Ponte, R. M. & Heimback, P. (2008a). Sea surface temperature budgets and mechanisms controlling upper ocean climate variability. *Proceedings of ASLO/AGU/TOS Ocean Science Meeting*, Orlando, FL, March 2008.

Vinogradova N. T.; Zaccheo, T. S., Alcala, C. M. & Vandemark, D. (2008b). Regional fused sea surface temperature system for the Gulf of Maine. *Proceedings of IEEE International Geoscience & Remote Sensing Symposium (IGARSS)*, Boston, MA, July 2008.

Vinogradova, N. T. & Ponte, R. M. (2009). Dynamics and forcing of upper ocean heat balance on climate scales. In preparation.

Vinogradova, N. T.; Vinogradov S. V., Nechaev D. A., Kamenkovich V.M., Blumberg, A. F., Ahsan Q. & Li, H. (2005). Evaluation of the Northern Gulf of Mexico Littoral Initiative (NGLI) model based on the observed temperature and salinity in the Mississippi Bight, *MTS Journal,* 38(2), 25-38.

Wang, W. & McPhaden, M. J. (1999). The surface-layer heat balance in the Equatorial Pacific ocean. Part I: mean seasonal cycle. *J. Phys. Oceanogr.*, 29, 1812-1831

Wunsch, C.; Hemibach, P., Ponte, R.M., & Fukumori, I. (2009). The global general circulation of the oceans estimated by the ECCO-consortium. *Oceanography*, 22, 88-103.

Xue H.; Chei, F. & Pettigrew, N. R. (2000). A model study of the seasonal circulation in the Gulf of Maine. *J. Phys. Oceanogr.*, 30, 1111-1135

Xue, H..; Li, L., Cousins, S., & Pettigrew, N. R. (2005). The GoMOOS nowcast/forecast system. *Cont. Shelf. Res.*, 25. 2122-2146.

Geoscience and Remote Sensing

Edited by Pei-Gee Peter Ho

ISBN 978-953-307-003-2
Hard cover, 598 pages
Publisher InTech
Published online 01, October, 2009
Published in print edition October, 2009

Remote Sensing is collecting and interpreting information on targets without being in physical contact with the objects. Aircraft, satellites ...etc are the major platforms for remote sensing observations. Unlike electrical, magnetic and gravity surveys that measure force fields, remote sensing technology is commonly referred to methods that employ electromagnetic energy as radio waves, light and heat as the means of detecting and measuring target characteristics. Geoscience is a study of nature world from the core of the earth, to the depths of oceans and to the outer space. This branch of study can help mitigate volcanic eruptions, floods, landslides ... etc terrible human life disaster and help develop ground water, mineral ores, fossil fuels and construction materials. Also, it studies physical, chemical reactions to understand the distribution of the nature resources. Therefore, the geoscience encompass earth, atmospheric, oceanography, pedology, petrology, mineralogy, hydrology and geology. This book covers latest and futuristic developments in remote sensing novel theory and applications by numerous scholars, researchers and experts. It is organized into 26 excellent chapters which include optical and infrared modeling, microwave scattering propagation, forests and vegetation, soils, ocean temperature, geographic information , object classification, data mining, image processing, passive optical sensor, multispectral and hyperspectral sensing, lidar, radiometer instruments, calibration, active microwave and SAR processing. Last but not the least, this book presented chapters that highlight frontier works in remote sensing information processing. I am very pleased to have leaders in the field to prepare and contribute their most current research and development work. Although no attempt is made to cover every topic in remote sensing and geoscience, these entire 26 remote sensing technology chapters shall give readers a good insight. All topics listed are equal important and significant.

InTech Europe
University Campus STeP Ri
Slavka Krautzeka 83/A

InTech China
Unit 405, Office Block, Hotel Equatorial Shanghai
No.65, Yan An Road (West), Shanghai, 200040, China

51000 Rijeka, Croatia
Phone: +385 (51) 770 447
Fax: +385 (51) 686 166
www.intechopen.com

中国上海市延安西路65号上海国际贵都大饭店办公楼405单元
Phone: +86-21-62489820
Fax: +86-21-62489821

IntechOpen

IntechOpen